Clinical Evaluation of Zero-Echo-Time Attenuation Correction for Brain ^{18}F-FDG PET/MRI: Comparison with Atlas Attenuation Correction

Tetsuro Sekine[1,2], Edwin E.G.W. ter Voert[1], Geoffrey Warnock[1,3,4], Alfred Buck[1], Martin Huellner[1,5], Patrick Veit-Haibach[1,6], and Gaspar Delso[7]

[1]Department of Nuclear Medicine, University Hospital Zurich, Zurich, Switzerland; [2]Department of Radiology, Nippon Medical School, Tokyo, Japan; [3]Institute of Pharmacology & Toxicology, University of Zurich, Zurich, Switzerland; [4]PMOD Technologies Ltd., Zurich, Switzerland; [5]Department of Neuroradiology, University Hospital Zurich, Zurich, Switzerland; [6]Division of Diagnostic and Interventional Radiology, Department of Medical Radiology, University Hospital Zurich, Zurich, Switzerland; and [7]GE Healthcare Waukesha, Wisconsin

Accurate attenuation correction (AC) on PET/MR is still challenging. The purpose of this study was to evaluate the clinical feasibility of AC based on fast zero-echo-time (ZTE) MRI by comparing it with the default atlas-based AC on a clinical PET/MR scanner. **Methods:** We recruited 10 patients with malignant diseases not located on the brain. In all patients, a clinically indicated whole-body ^{18}F-FDG PET/CT scan was acquired. In addition, a head PET/MR scan was obtained voluntarily. For each patient, 2 AC maps were generated from the MR images. One was atlas-AC, derived from T1-weighted liver acquisition with volume acceleration flex images (clinical standard). The other was ZTE-AC, derived from proton-density-weighted ZTE images by applying tissue segmentation and assigning continuous attenuation values to the bone. The AC map generated by PET/CT was used as a silver standard. On the basis of each AC map, PET images were reconstructed from identical raw data on the PET/MR scanner. All PET images were normalized to the SPM5 PET template. After that, these images were qualified visually and quantified in 67 volumes of interest (VOIs; automated anatomic labeling, atlas). Relative differences and absolute relative differences between PET images based on each AC were calculated. ^{18}F-FDG uptake in all 670 VOIs and generalized merged VOIs were compared using a paired *t* test. **Results:** Qualitative analysis shows that ZTE-AC was robust to patient variability. Nevertheless, misclassification of air and bone in mastoid and nasal areas led to the overestimation of PET in the temporal lobe and cerebellum (%diff of ZTE-AC, 2.46% ± 1.19% and 3.31% ± 1.70%, respectively). The |%diff| of all 670 VOIs on ZTE was improved by approximately 25% compared with atlas-AC (ZTE-AC vs. atlas-AC, 1.77% ± 1.41% vs. 2.44% ± 1.63%, $P < 0.01$). In 2 of 7 generalized VOIs, |%diff| on ZTE-AC was significantly smaller than atlas-AC (ZTE-AC vs. atlas-AC: insula and cingulate, 1.06% ± 0.67% vs. 2.22% ± 1.10%, $P < 0.01$; central structure, 1.03% ± 0.99% vs. 2.54% ± 1.20%, $P < 0.05$). **Conclusion:** The ZTE-AC could provide more accurate AC than clinical atlas-AC by improving the estimation of head–skull attenuation. The misclassification in mastoid and nasal areas must be addressed to prevent the overestimation of PET in regions near the skull base.

Received Mar. 8, 2016; revision accepted May 31, 2016.
For correspondence or reprints contact: Tetsuro Sekine, University Hospital Zurich, Ramistrasse 100, 8091, Zurich, Switzerland.
E-mail: tetsuro.sekine@gmail.com
Published online Jun. 23, 2016.

Key Words: PET/MR; attenuation correction; atlas-based; brain; ^{18}F-FDG; ZTE

J Nucl Med 2016; 57:1927–1932
DOI: 10.2967/jnumed.116.175398

Integrated PET/MR systems were commercially developed by 2 vendors—Siemens Healthcare, the Biograph mMR in 2011, and GE Healthcare, the SIGNA PET/MR in 2014—and have been introduced in many institutions (more than 90 in the world). Previous studies have revealed that PET/MR provides good performance in the investigation of brain function, tumor, and degenerative diseases (*1*). The combined MRI system not only delivers detailed brain anatomy, but also can make PET image quality better by correcting partial-volume effects or motion artifacts (*2,3*). In addition, radiation exposure derived from CT scans was saved by replacing CT with MRI. However, several technical challenges remain before the full performance of PET/MR can be exploited. One of the important drawbacks to be improved is that of attenuation correction (AC) using MR imaging data (*4*). Unlike conventional PET systems, it is difficult to implement CT or rotating point sources in PET/MR systems, because of the high magnetic field. Furthermore, the information typically derived from conventional MR imaging is a mixture of proton density and relaxation properties, which does not correlate with γ-ray attenuation. To overcome this drawback, vendors and researchers have proposed several novel AC methods (*4*). These MR-based AC methods are roughly classified into 3 families, as well as combinations thereof. The first family is that of template-/atlas-/model-based approaches (*5–7*). The second one is that of segmentation approaches (*8–12*). The third one constitutes methods directly estimating attenuation information from emission data (*13,14*).

For clinical use, both mMR and SIGNA have Dixon-based 4-class segmentation approaches (i.e., air, lung, fat, and soft tissue). However, these methods are not recommended for brain studies, because neglecting bone introduces a significant bias in the area of the cortex (*15*). In addition, the mMR has a clinical dual ultrashort echo (UTE)–based segmentation method (*8*) and a prototype model–based method (*7*). In turn, the SIGNA has a clinical atlas-based

method and a prototype zero-echo-time (ZTE)–based segmentation method (*5,16,17*). The clinical atlas-AC on SIGNA is comparatively accurate in supratentorial regions, whereas not accurate enough in the infratentorial regions (*5*). It therefore needs to be improved. ZTE-AC is a promising new technique that offers a potential solution to these limitations. The ZTE MR sequence is well suited to achieve a proton-density contrast, which is ideal for bone tissue segmentation.

The first 2 reports dealing with ZTE MR imaging revealed its potential for accurate tissue classification (*16,17*). However, these reports did not perform a clinical PET evaluation of ZTE-AC. Also, the acquisition times of ZTE in these studies are too long to be used in a clinical setting (>2 min).

The aim of this paper was to clarify the clinical feasibility of attenuation correction based on fast-acquisition ZTE by comparing it with the current clinical MR-based AC method, atlas-based AC, and with the silver standard, CT-based AC method.

MATERIALS AND METHODS

This study was approved by the institutional review board. All subjects provided a signed informed consent form before the examinations. All experiments were performed in accordance with relevant guidelines and regulations.

Patients

We recruited 10 patients (5 men, 5 women; median age, 64 y; age range, 37–80 y). These patients were completely different from those of previous studies (*5,18*).

PET/CT and PET/MR Examination

The PET/CT acquisition followed the standard protocol for a clinical oncology study (Discovery 690 time-of-flight [TOF] PET/CT; GE Healthcare). The average injected dose of ^{18}F-FDG was 234 ± 49.6 MBq (range, 179–307 MBq) in accordance with clinical guidelines (*19*). First, a helical whole-body CT scan (120 kV; 15–80 mA with automatic dose modulation; rotation time, 0.5 s; helical thickness, 3.75 mm; pitch, 39.37 mm/rot; matrix size, 512 × 512; slice thickness, 3.3 mm; pixel dimensions, 1.4 × 1.4 mm^2) was acquired for AC of PET data and diagnostic purposes (*20*). Subsequently, a whole-body PET dataset including the head was acquired. Immediately before or after the PET/CT scan, patients were transferred to the integrated TOF PET/MR scanner (SIGNA PET/MR; GE Healthcare), and a brain PET/MR scan was obtained as part of the study examination. A 2-min PET scan with a standard head coil (8-channnel HD Brain; GE Healthcare) was acquired. The PET/MR scan was acquired at 128.0 ± 37.4 min after tracer injection.

During the PET acquisition on the PET/MR, GE–liver acquisition with volume acceleration flex (LAVA-Flex) T1-weighted (T1w) images (axial acquisition: repetition time, ~4 ms; echo time, 2.23 ms; flip angle, 5°; slice thickness, 5.2 mm, with 2.6-mm overlap; 120 slices; pixel size, 1.95 × 1.95 mm^2; number of excitations, 0.9; acquisition time, 18 s) were acquired for atlas-AC. These parameters were identical to the previous study except for the flip angle (5° in the current study, 12° in the previous study) (*5*). The change of the flip angle used in the default AC acquisition was introduced by the manufacturer soon after the deployment of the first clinical systems. The version finally approved by the Food and Drug Administration uses a 5° flip angle.

Additionally, proton-density ZTE MR images (sagittal acquisition; nonselective hard pulse excitation; 3-dimensional center-out radial acquisition; repetition time, ~410 ms; nominal echo time, 0 ms; transmit-receive switching times, ~20 μs; flip angle, 1°; slice thickness, 2.78 mm; 118 slices; pixel size, 1.17 × 1.17 mm^2; bandwidth ± 62.5 kHz; number of excitations, 4; acquisition time, 48 s; spokes per segment, 512) were acquired. The ZTE scan was accelerated by reducing the resolution with respect to previous studies, to achieve a clinically efficient scan duration (*16*). This prototype ZTE sequence is not a commercial product.

Reconstruction of AC Map

For each patient, 3 AC maps were generated on the basis of each of the atlas-AC, ZTE-AC, and CT-AC methods.

Attenuation Map Based on Atlas Method

The atlas-AC map was generated from the LAVA-Flex T1w images using a proprietary process that consists of 4 main steps. First, Hessian bone enhancement from LAVA-FLEX T1w images is performed. Second, a pseudo-CT is generated by rigid and nonrigid B-spline elastic registration between the enhanced images and a CT-based head atlas. This atlas is provided by the manufacturer. Third, the attenuation map is generated from the pseudo-CT using the standard energy conversion and resampling. Finally, the MR hardware, coil, and bed are added to the attenuation map. This entire procedure takes less than 30 s and requires no user interaction. A more detailed description of the algorithm is provided in Wollenweber et al. (*20*).

Attenuation Map Based on ZTE Imaging

The processing steps detailed below were performed using custom Matlab scripts (version 7.11.0; The MathWorks). The process consists of 3 main steps as below. First, bias correction was applied (*21*). Second, tissue classification was performed by applying simple thresholding for soft tissue/bone and bone/air, based on the values of the tissue and air histogram peaks. We applied the thresholds directly to the ZTE data (without log-scaling). The air threshold was 0.25 and bone threshold 0.85. Third, continuous attenuation values were assigned to the bone tissue, based on the linear correlation between CT and ZTE MR values (offset, 300; slope, 2,400; maximum bone value, 2,000 Hounsfield units). To the soft tissue, a fixed attenuation value of 42 Hounsfield units was assigned. The formulas to generate the thresholds and attenuation value were defined empirically before the study and remained constant for all patients. The computation time is less than 30 s on a standard desktop computer. A more detailed description of the algorithm is provided in Wiesinger et al. (*16*).

Coregistered Attenuation Map Based on CT Method

The processing steps detailed below were performed using custom Matlab scripts and PMOD (version 3.6; PMOD Technologies Ltd.). The coregistered CT-AC map was generated as follows. First, the original head CT was exported from the PET/CT scanner and converted into AC-map using a Matlab version of the same bilinear mapping implemented in the SIGNA PET/MRI. Second, from this map, the CT table was removed manually. Third, a threshold was set to extract the outside air component from the CT-AC map. None of the images used in this study contained artifacts likely to affect air thresholding. Fourth, a normalized mutual information matching algorithm (PMOD) was used to derive the registration parameters necessary to match CT to LAVA-Flex T1w, and the final matching was performed using custom Matlab routines. Finally, the CT-AC map was superimposed on the atlas-AC map, thereby replacing it (*5*).

Reconstruction of PET Images

Only the list-mode raw PET data from the TOF PET/MR examination were used. PET images were reconstructed with AC based on each of the 3 attenuation maps and the following parameters: fully 3-dimensional ordered-subset expectation maximization iterative reconstruction; subsets, 28; iterations, 8; pixel size, 1.17 × 1.17 mm^2; point spread function modeling; transaxial postreconstruction gaussian filter cutoff, 3 mm; axial filter, 1:4:1; scatter; normalization; dead-time and decay corrections; TOF reconstruction.

Analysis

All PET images were spatially normalized to a brain template (SPM5; University College London), and 67 automated anatomic labeling (AAL) volumes of interest (VOIs) were applied (Supplemental Fig. 1; supplemental materials are available at http://jnm.snmjournals.org). In each VOI, ^{18}F-FDG uptake values from CT-AC (PET_{CT}), atlas-AC (PET_{atlas}), and ZTE-AC (PET_{ZTE}) were measured. Each matching AC map was also normalized using the same transformation generated during the normalization of the PET.

Qualitative Analysis

Relative difference (%diff) images of PET ($PET_{atlas/ZTE}$ minus PET_{CT}, divided by PET_{CT}, times 100) and difference imaging of AC-map (the attenuation value of atlas-AC/ZTE-AC minus that of CT-AC) ($diff_{map}$) were generated for each patient. From all 10 patients, the average and SD of each %diff of PET and $diff_{map}$ were subsequently generated and visually assessed.

Quantitative Analysis

In the 67 AAL VOIs of each of the 10 patients (670 VOIs in total), Bland–Altman analysis was performed by calculating %diff of both atlas and ZTE. The |%diff| was also calculated.

To assess the error distribution in the brain, the 67 AAL VOIs were merged into 7 more generalized VOIs: frontal lobes, occipital lobes, parietal lobes, insula and cingulate gyrus, central structures (caudate nucleus, putamen, pallidum, and thalamus), temporal lobes, and cerebellum (Supplemental Fig. 2). The %diff and |%diff| were calculated in each merged region. All image analyses were performed using PMOD 3.6.

Statistical significance was assessed using a paired *t* test. For the comparison of |%diff|, 1-tailed testing was used to know which one was superior and closer to zero. And for the comparison in each merged region, Bonferroni adjustment was used. A *P* value of less than 0.05 was deemed statistically significant. All statistical analyses used SPSS Statistics (version 19.0.0; IBM).

RESULTS

All 10 patients successfully underwent PET/CT and PET/MR examinations. A representative case is given in Figure 1.

Qualitative Analysis

In qualitative analysis, several features on each AC were observed. On $diff_{map}$ of atlas-based AC, registration inaccuracies and the systematic underestimation of the skull, especially in temporal bone and skull base, were observed (top and second row, Figure 2A). On atlas-AC PET, the error in superior cerebrum was small (top row, Fig. 2B) contrary to relatively large error on atlas-AC (top row, Fig. 2A). The explanation could be that some of the registration inaccuracy on atlas-AC was compensated in superior cerebrum by mutually cancelling under- and overestimation. The bias in regions adjacent to underestimated bone was pronounced, especially in inferior cerebrum and cerebellum (top row, Fig. 2B).

On $diff_{map}$ of ZTE-based AC, subtle underestimation of superior cranium and overestimation of mastoid and nasal areas were found (third row, Fig. 2A). In the case of the sinus region, this overestimation was due to misclassification of air/soft-tissue interfaces as bone (Fig. 1B). ZTE-AC was much more robust to patient variability than atlas-AC, as shown by the SD of the error in the cranium (fourth row vs. second row, Fig. 2A). On ZTE AC PET, subtle underestimation of superior cerebrum and overestimation of temporal lobes and cerebellum were shown, which is consistent with attenuation map errors (third row, Fig. 2B). Detailed explanations of the figures are provided in the figure legend.

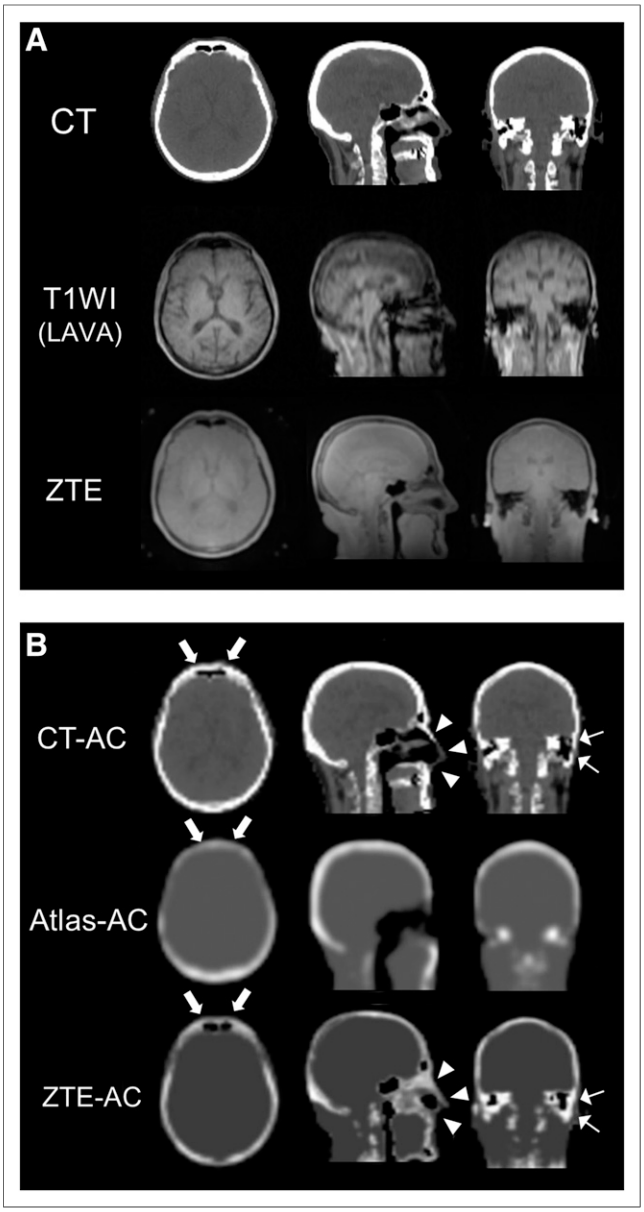

FIGURE 1. A representative case. (A) CT, T1w LAVA-Flex, and proton-density-weighted ZTE MR images are shown. (B) From each set of source images, 3 different attenuation maps were generated. Frontal sinus is not visible on atlas-AC (arrows, B). In nasal and mastoid areas, misclassification of bone is pronounced on ZTE-AC (arrowheads and thin arrows, B).

Quantitative Analysis

Though the Bland–Altman plot for all 670 VOIs proved that ZTE tends to overestimate on some regions, globally no bias and no systematic under- or overestimation ($-0.09\% \pm 2.26\%$; range, -4.74%–7.99%) were observed. These results are superior to those of atlas-AC ($-1.71\% \pm 2.38\%$; range, -7.39%–8.00%) (Fig. 3). Furthermore, the average |%diff| of the 670 VOIs with ZTE-AC was significantly smaller than atlas-AC by 25% (ZTE-AC vs. atlas-AC; $1.77\% \pm 1.41\%$ vs. $2.44\% \pm 1.63\%$, $P < 0.01$, Table 1).

In generalized VOIs, the underestimation with atlas-AC was pronounced in regions close to the skull base, such as the temporal lobes ($-2.67\% \pm 2.07\%$) and cerebellum ($-3.64\% \pm 2.65\%$). In contrast, the overestimation with ZTE-AC was found in these

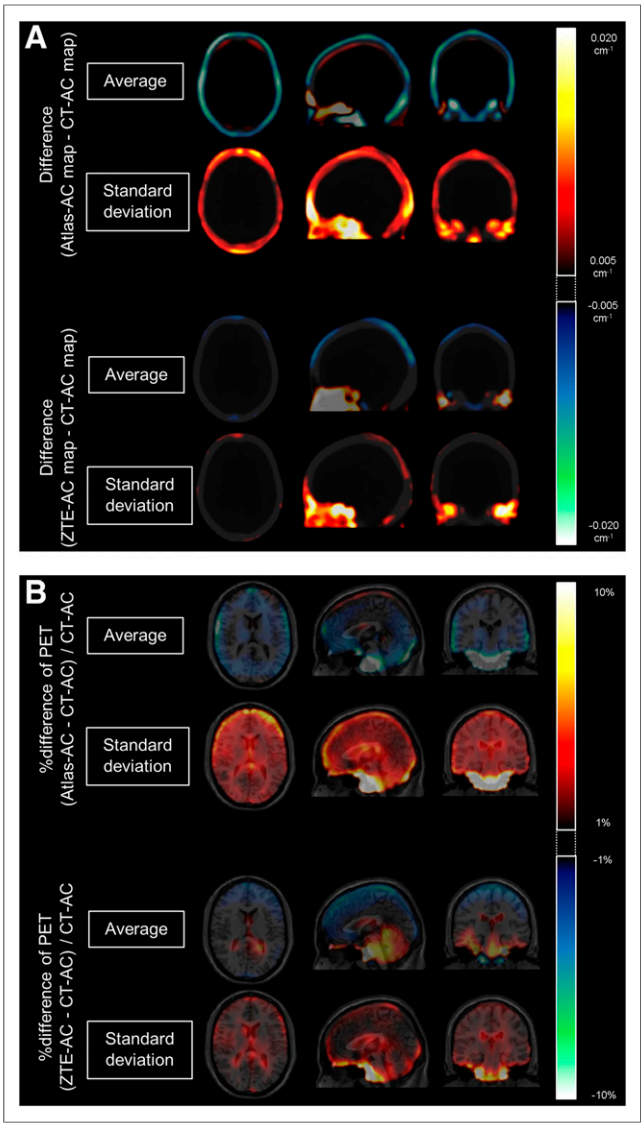

FIGURE 2. Average and SD images, from all 10 patients after normalization. $diff_{map}$ (A) and %diff of PET (B) are shown. On atlas-AC, registration errors can be appreciated as overestimation of inner side of skull and underestimation of outer side (top row, A). Also, there is systematic underestimation of skull, especially in temporal bone and skull base (top row, A). On ZTE-AC, subtle underestimation of superior cranium and overestimation of mastoid and nasal areas can be appreciated (third row, A). ZTE-AC is much more robust to patient variability than atlas-AC (fourth row vs. second row, A). (B) PET results are in agreement with these AC-map results.

regions (%diff: temporal lobes, 2.46% ± 1.19%, $P < 0.01$; cerebellum, 3.31% ± 1.70%, $P < 0.01$, Table 2). The absolute errors with ZTE-AC were significantly smaller than those with atlas-AC in the region of insula and cingulate (1.06% ± 0.67% vs. 2.22% ± 1.10%; $P < 0.01$) and central structure (1.03% ± 0.99% vs. 2.54% ± 1.20%; $P < 0.05$) (Table 2).

DISCUSSION

In this study, we evaluated the clinical feasibility of an attenuation-correction method based on prototype proton-density-weighted ZTE by comparing it to the default atlas-based AC method currently used by the SIGNA PET/MR. Clinical data from PET/CT patients volunteering for an additional PET/MR acquisition were used for this study.

The overall ^{18}F-FDG uptake bias of ZTE-AC was 25% lower than that of atlas-AC. This improvement was achieved by the improved registration and assignment of correct attenuation values for the skull. Especially in central structures and insula and cingulate areas, a significant improvement with ZTE-AC was found in comparison to clinical atlas-AC. On the other hand, ZTE-AC was found to misclassify some of the nasal and mastoid areas as bone, which caused overestimation of ^{18}F-FDG uptake in the temporal lobe and cerebellum.

In our study, the relative error and absolute relative error of ZTE-AC across all 670 VOIs were −0.09% ± 2.26% and 1.77% ± 1.41%, respectively, which are generally comparable to other studies (*9,22–24*). Previously reported absolute relative percentage errors of PET images range from 1.38% ± 4.52% to 2.55% ± 0.86% (*9,22–24*), though care should be taken when comparing these studies and the present study, because of analysis variations. Also, the use of TOF in our study has a potential to compensate the AC inconsistencies, causing the bias in the reconstructed PET images to spread over a larger area (*13,18,25,26*).

Previous studies with 15 clinical datasets—acquired with a PET/CT + MR trimodality setup—concluded that skull-bone identification based on a ZTE sequence is expected to have sufficient anatomic accuracy for PET AC (*17*). Though the acquisition time is accelerated in this study (172 s → 48 s) with lower spatial resolution (1.4 × 1.4 × 1.4 → 1.17 × 1.17 × 2.78 mm) to meet clinical requirements, accurate segmentation was also obtained in the current study, as shown in Figure 2A, in which the average and the SD of bone attenuation error from all 10 patients were much smaller than with atlas-AC. The improvement with ZTE-AC was noticeable in the inferior cerebrum, which reflects the correct estimation of temporal bone. The thin temporal bone causes misclassification and systematic underestimation by atlas-AC, which leads to the underestimation of ^{18}F-FDG uptake in the same axial slices, along those lines of response (*5*). These results are consistent with the expectations for ZTE-based AC, and in particular its feature of providing measurement-based bone density information, rather than estimates based on a priori models.

In contrast, the misclassification and systematic overestimation of nasal and mastoid areas were observed (third row, Fig. 2A), leading to the overestimation of uptake in the cerebellum and temporal lobes. This issue should definitely be addressed, because the cerebellum is sometimes used as a reference for the normalization of the whole brain and the temporal lobes are one of the most

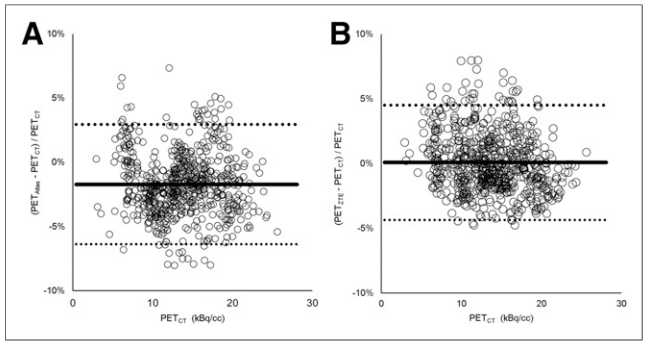

FIGURE 3. Bland–Altman plots of atlas-AC (A) and ZTE-AC (B) for 67 VOIs. *10 patients.

TABLE 1
%diff and |%diff| in ^{18}F-FDG Uptake (kBq/mL) Between CT-AC and Atlas-AC/ZTE-AC in All Regions ($67 \times 10 = 670$ VOIs)

Parameter	Mean ± SD
%diff on atlas	−1.71% ± 2.38%
%diff on ZTE*	−0.09% ± 2.26%
|%diff| on atlas	2.44% ± 1.63%
|%diff| on ZTE*	1.77% ± 1.41%

%diff is atlas-AC/ZTE-AC minus CT-AC, divided by CT-AC. |%diff| is absolute value of %diff.
*Atlas-AC vs. ZTE-AC, $P < 0.01$.

important regions when dementia studies are performed. This is a known issue, caused by the discontinuous mapping of ZTE intensities to attenuation values. It affects primarily interfaces between soft tissue and air, in which partial-volume effects lead to averaged values that fall within the intensity range assigned to bone (*16,17*).

To improve this drawback, there are several options. One is the investigation of acceleration techniques allowing the saved scan time to be invested in improving the spatial resolution, hence reducing partial-volume effects. A second option is the use of more advanced segmentation approaches, capable of using local neighborhood information to identify partial-volume effects (e.g., machine-learning method (*27*)). Alternatively, with knowledge-based approaches, anatomic priors can be used to drive dedicated classification approaches in different anatomic regions (*28*). One potential drawback of such hybrid methods—aside from the increased computational cost—is losing the ability to adapt to off-norm anatomies, one of the main advantages of measurement-based methods over model-based ones. Further study is needed to improve the sinus and mastoid areas, to take full advantage of ZTE-based AC.

Following are additional features of the ZTE-AC methods. First, there was systematic underestimation of the superior cranium, which caused subtle underestimation of ^{18}F-FDG uptake close to these areas. We assume that this problem is due to the partial-volume effect of the thin cortical bone in these regions. Second, ZTE requires minimal gradient switching, which can reduce eddy current effect. This might be some advantage when compared with the UTE-AC, which is one of the most popular segmentation-based methods in clinical head PET/MR study (*8*). The artifact sometimes causes the error in the calculation of T2 relaxation time on UTE-AC because of reduced signal intensities in the first UTE echo just after switching (*9,29*). There is no fair-comparison study between UTE-AC and ZTE-AC in the clinical setting because each method has been developed by a different vendor. Third, the absence of preparation pulses or multiple echoes makes ZTE a time-efficient acquisition (i.e., most of the repetition time is used to acquire data) and suitable for routine clinical use. Indeed, on PET/MR, the total MR acquisition time is generally longer than that of PET, and any options to minimize or accelerate MR acquisition time should be considered (*30*). Fourth, the current ZTE-AC has the capability of assigning continuous attenuation values to bone tissue, rather than discrete ones. Two previous studies estimate the negative effect of segmentation-based AC methods with discrete bone attenuation, using simulated CT images. Even if the classification of the bone/soft-tissue component is completely precise, the PET bias is within ±10% in one study and is 4.0% ± 3.7% in the other study (*11,31*). Also, several studies revealed that adding the continuous bone attenuation value calculated from T2 relaxation time using dual UTE sequences contributes to improve AC (*9,10,31*).

From the view of the comparison between atlas-/template-/model-based methods and segmentation methods, the former have 2 inherent limitations. One is that they cannot accurately detect the cavity of the sinus because there is wide interpatient variability. In our cohort, the sinus in the frontal bone is more precisely detected by ZTE-AC than atlas-AC (Figs. 1B and 2A). The other is that these methods are not suitable for patients with abnormal anatomy or surgical alterations. Though this topic is out of the scope for this study, ZTE-AC has the potential to detect these off-norm features precisely (*16*). On the other hand, segmentation-based methods are more sensitive to measurement artifacts, such as those caused by certain metallic implants. Ideally, both atlas-/template-/model-based methods and segmentation methods should be available in a clinical scanner.

Other additional features and advantages of this study are as follows.

First, we performed the assessment using real TOF PET/MR scanner data, not simulation data (e.g., combining PET/CT data with MRI data). In our study, we used a state-of-the-art TOF PET/MR system, consisting of silicon photomultipliers with less than

TABLE 2
%diff and |%diff| in ^{18}F-FDG Uptake (kBq/mL) Between Atlas-/ZTE-AC and CT-AC in Each Merged Region

Parameter	Frontal lobe	Occipital lobe	Parietal lobe	Insula and cingulate	Central structure	Temporal lobe	Cerebellum
%diff on atlas-AC	−1.17% ± 2.61%	−1.64% ± 1.41%	−1.20% ± 1.76%	−1.10% ± 2.31%	−1.83% ± 2.21%	−2.67% ± 2.07%	−3.64% ± 2.65%
%diff on ZTE-AC	−1.57% ± 1.25%	0.05% ± 0.89%*	−1.59% ± 1.10%	−0.55% ± 1.17%	0.54% ± 1.35%*	2.46% ± 1.19%*	3.31% ± 1.70%*
|%diff| on atlas-AC	2.42% ± 1.35%	1.66% ± 1.39%	1.63% ± 1.32%	2.22% ± 1.10%	2.54% ± 1.20%	2.78% ± 1.90%	3.73% ± 2.51%
|%diff| on ZTE-AC	1.75% ± 0.95%	0.64% ± 0.58%	1.70% ± 0.89%	1.06% ± 0.67%*	1.03% ± 0.99%†	2.46% ± 1.19%	3.31% ± 1.70%

%diff is atlas-AC/ZTE-AC minus CT-AC divided by CT-AC. |%diff| is absolute value of %diff.
atlas-AC vs. ZTE-AC, *$P < 0.05$, †$P < 0.01$.

400-ps temporal resolution, enabling TOF acquisition (*32*). Evaluating the clinical feasibility of a new AC method is desirable in this realistic setting.

Second, we compared ZTE-AC with the atlas-AC currently used in clinical practice. If only 1 method were compared with the standard of reference in a small sample, the results may highly depend on interindividual variability. Hence, the comparison with current clinical methods on PET/MR scanners is mandatory.

Third, through the use of a widely available brain template (AAL), our results can be readily applied to another dataset or used in other centers (*33*).

A limitation of our study is the small number of patients considered. However, using automated methods and comparing 2 AC methods (atlas-AC and ZTE-AC) against a silver standard (CT-AC), we aimed to reduce bias. Also, the PET acquisition was not ideal for a brain PET scan: the scan duration was relatively short, 2 min, leading to a decrease in the signal to noise of the PET images. However, performing the analysis on a regional level (AAL VOI) reduced the sensitivity to the noise at the voxel level.

CONCLUSION

Short acquisition proton-density-weighted ZTE MR imaging can provide accurate attenuation maps for advanced quantitative brain studies. However, the overestimation of mastoid and nasal areas must be addressed to take full advantage of this new technique.

The errors introduced using ZTE-AC on TOF PET/MR data did not exceed 8% in any automated anatomic labeling brain VOIs. This error was approximately 25% smaller than that of the clinically used atlas-based AC method.

DISCLOSURE

The costs of publication of this article were defrayed in part by the payment of page charges. Therefore, and solely to indicate this fact, this article is hereby marked "advertisement" in accordance with 18 USC section 1734. Patrick Veit-Haibach received IIS grants from Bayer Healthcare, Roche Pharmaceutical, GE Healthcare, and Siemens Medical Solutions and speaker fees from GE Healthcare. Gaspar Delso is an employee of GE Healthcare. Only non-GE employees had control of inclusion of data and information that might present a conflict of interest for authors who are employees of GE Healthcare. No other potential conflict of interest relevant to this article was reported.

REFERENCES

1. Nensa F, Beiderwellen K, Heusch P, Wetter A. Clinical applications of PET/MRI: current status and future perspectives. *Diagn Interv Radiol.* 2014;20:438–447.
2. Grimm R, Furst S, Souvatzoglou M, et al. Self-gated MRI motion modeling for respiratory motion compensation in integrated PET/MRI. *Med Image Anal.* 2015;19:110–120.
3. Acosta O, Bourgeat P, Zuluaga MA, et al. Automated voxel-based 3D cortical thickness measurement in a combined Lagrangian-Eulerian PDE approach using partial volume maps. *Med Image Anal.* 2009;13:730–743.
4. Mehranian A, Arabi H, Zaidi H. Vision 20/20: magnetic resonance imaging-guided attenuation correction in PET/MRI—challenges, solutions, and opportunities. *Med Phys.* 2016;43:1130–1155.
5. Sekine T, Buck A, Delso G, et al. Evaluation of atlas-based attenuation correction for integrated PET/MR in human brain: application of a head atlas and comparison to true CT-based attenuation correction. *J Nucl Med.* 2016;57: 215–220.
6. Rota Kops E, Hautzel H, Herzog H, Antoch G, Shah NJ. Comparison of template-based versus CT-based attenuation correction for hybrid MR/PET scanners. *IEEE Trans Nucl Sci.* 2015;62:2115–2121.
7. Koesters T, Friedman KP, Fenchel M, et al. Dixon sequence with superimposed model-based bone compartment provides highly accurate PET/MR attenuation correction of the brain. *J Nucl Med.* 2016;57:918–924.
8. Aasheim LB, Karlberg A, Goa PE, et al. PET/MR brain imaging: evaluation of clinical UTE-based attenuation correction. *Eur J Nucl Med Mol Imaging.* 2015;42:1439–1446.
9. Juttukonda MR, Mersereau BG, Chen Y, et al. MR-based attenuation correction for PET/MRI neurological studies with continuous-valued attenuation coefficients for bone through a conversion from R2* to CT-Hounsfield units. *Neuroimage.* 2015;112:160–168.
10. Cabello J, Lukas M, Forster S, Pyka T, Nekolla SG, Ziegler SI. MR-based attenuation correction using ultrashort-echo-time pulse sequences in dementia patients. *J Nucl Med.* 2015;56:423–429.
11. Catana C, van der Kouwe A, Benner T, et al. Toward implementing an MRI-based PET attenuation-correction method for neurologic studies on the MR-PET brain prototype. *J Nucl Med.* 2010;51:1431–1438.
12. Keereman V, Fierens Y, Broux T, De Deene Y, Lonneux M, Vandenberghe S. MRI-based attenuation correction for PET/MRI using ultrashort echo time sequences. *J Nucl Med.* 2010;51:812–818.
13. Boellaard R, Hofman MB, Hoekstra OS, Lammertsma AA. Accurate PET/MR quantification using time of flight MLAA image reconstruction. *Mol Imaging Biol.* 2014;16:469–477.
14. Rezaei A, Defrise M, Nuyts J. ML-reconstruction for TOF-PET with simultaneous estimation of the attenuation factors. *IEEE Trans Med Imaging.* 2014;33:1563–1572.
15. Andersen FL, Ladefoged CN, Beyer T, et al. Combined PET/MR imaging in neurology: MR-based attenuation correction implies a strong spatial bias when ignoring bone. *Neuroimage.* 2014;84:206–216.
16. Wiesinger F, Sacolick LI, Menini A, et al. Zero TE MR bone imaging in the head. *Magn Reson Med.* 2016;75:107–114.
17. Delso G, Wiesinger F, Sacolick LI, et al. Clinical evaluation of zero-echo-time MR imaging for the segmentation of the skull. *J Nucl Med.* 2015;56:417–422.
18. Sekine T, Burgos N, Warnock G, et al. Multi atlas-based attenuation correction for brain FDG-PET imaging using a TOF-PET/MR scanner- comparison with clinical single atlas- and CT-based attenuation correction. *J Nucl Med.* March 24, 2016 [Epub ahead of print].
19. Boellaard R, O'Doherty MJ, Weber WA, et al. FDG PET and PET/CT: EANM procedure guidelines for tumour PET imaging: version 1.0. *Eur J Nucl Med Mol Imaging.* 2010;37:181–200.
20. Wollenweber SD, Ambwani S, Delso G, et al. Evaluation of an atlas-based PET head attenuation correction using PET/CT & MR patient data. *IEEE Trans Nucl Sci.* 2013;60:3383–3390.
21. Tustison NJ, Avants BB, Cook PA, et al. N4ITK: improved N3 bias correction. *IEEE Trans Med Imaging.* 2010;29:1310–1320.
22. Izquierdo-Garcia D, Hansen AE, Forster S, et al. An SPM8-based approach for attenuation correction combining segmentation and nonrigid template formation: application to simultaneous PET/MR brain imaging. *J Nucl Med.* 2014;55:1825–1830.
23. Poynton CB, Chen KT, Chonde DB, et al. Probabilistic atlas-based segmentation of combined T1-weighted and DUTE MRI for calculation of head attenuation maps in integrated PET/MRI scanners. *Am J Nucl Med Mol Imaging.* 2014;4:160–171.
24. Chen Y, Juttukonda M, Su Y, et al. Probabilistic air segmentation and sparse regression estimated pseudo CT for PET/MR attenuation correction. *Radiology.* 2015;275:562–569.
25. Davison H, Ter Voert EE, de Galiza Barbosa F, Veit-Haibach P, Delso G. Incorporation of time-of-flight information reduces metal artifacts in simultaneous positron emission tomography/magnetic resonance imaging: a simulation study. *Invest Radiol.* 2015;50:423–429.
26. Conti M. Why is TOF PET reconstruction a more robust method in the presence of inconsistent data? *Phys Med Biol.* 2011;56:155–168.
27. Santos Ribeiro A, Rota Kops E, Herzog H, Almeida P. Hybrid approach for attenuation correction in PET/MR scanners. *Nucl Instrum Methods Phys Res A.* 2014;734:166–170.
28. Wagenknecht G, Kops ER, Mantlik F, et al. Attenuation correction in MR-BrainPET with segmented T1-weighted MR images of the patient's head: a comparative study with CT. *IEEE Nucl Sci Symp Med Imaging Conf.* 2011:2261–2266.
29. Delso G, Carl M, Wiesinger F, et al. Anatomic evaluation of 3-dimensional ultrashort-echo-time bone maps for PET/MR attenuation correction. *J Nucl Med.* 2014;55:780–785.
30. Barbosa Fde G, von Schulthess G, Veit-Haibach P. Workflow in simultaneous PET/MRI. *Semin Nucl Med.* 2015;45:332–344.
31. Navalpakkam BK, Braun H, Kuwert T, Quick HH. Magnetic resonance-based attenuation correction for PET/MR hybrid imaging using continuous valued attenuation maps. *Invest Radiol.* 2013;48:323–332.
32. Surti S. Update on time-of-flight PET imaging. *J Nucl Med.* 2015;56:98–105.
33. Tzourio-Mazoyer N, Landeau B, Papathanassiou D, et al. Automated anatomical labeling of activations in SPM using a macroscopic anatomical parcellation of the MNI MRI single-subject brain. *Neuroimage.* 2002;15:273–289.